N O T I C E

THIS DOCUMENT HAS BEEN REPRODUCED FROM
MICROFICHE. ALTHOUGH IT IS RECOGNIZED THAT
CERTAIN PORTIONS ARE ILLEGIBLE, IT IS BEING RELEASED
IN THE INTEREST OF MAKING AVAILABLE AS MUCH
INFORMATION AS POSSIBLE

NASA TECHNICAL
MEMORANDUM

NASA TM-82406

PERFORMANCE OF PHOTOMULTIPLIER TUBES AND SODIUM IODIDE SCINTILLATION DETECTOR SYSTEMS

By Charles A. Meegan
Space Sciences Laboratory

March 1981

NASA

George C. Marshall Space Flight Center

Marshall Space Flight Center, Alabama

TABLE OF CONTENTS

PRECEDING PAGE BLANK NOT FILMED

LIST OF ILLUSTRATIONS

iv

LIST OF ILLUSTRATIONS (Concluded)

LIST OF TABLES

PERFORMANCE OF PHOTOMULTIPLIER TUBES AND SODIUM IODIDE SCINTILLATION DETECTOR SYSTEMS

I. INTRODUCTION

This report presents a discussion of the performance of photomultiplier tubes (PMT's) and NaI scintillation counters. The test procedures and described results were performed to evaluate detectors for use on the Burst and Transient Source Experiment (BATSE) on the Gamma Ray Observatory (GRO). These detectors consist of 50.8 cm (20 in.) diameter by 1.27 cm (0.5 in.) thick NaI crystals viewed by three photomultiplier tubes. An important goal of the tests was to determine the optimum shape for a light collector housing to optically couple the PMT's to the crystal.

Section II presents a general discussion of performance characteristics of photomultiplier tubes, NaI scintillators, and light collector housings. This section is intended to be of general interest to any user of scintillation detector systems. The following sections are more specific to our particular application. Section III describes procedures for measuring various parameters of detector systems, such as sensitivity, linearity, and energy resolution. Section IV presents the results of the tests for BATSE detectors. A brief summary of the conclusions is presented in Section V.

This report is concerned primarily with linearity and variance of detector pulse height distributions. Topics not covered include speed of PMT's, effects of magnetic fields, and temperature effects.

II. PERFORMANCE CHARACTERISTICS

An important parameter in these investigations is the relative variance V, which is a measure of the energy resolution of the detector. For any distribution in x, the relative variance is defined by

$$V = \left(\frac{\sigma_x}{\bar{x}}\right)^2 \quad ,$$

where $\bar{x}$ is the average value of x and σ_x is the standard deviation (root mean square deviation) of the distribution. The advantages in using relative variance to describe the width of a distribution are that it is

dimensionless and that it is additive when independent sources of variation are combined. Scintillation crystal manufacturers usually specify energy resolution R in terms of the full width at half maximum (FWHM) of a spectral line,

$$R = \frac{FWHM_x}{\bar{x}} \quad ,$$

generally expressed in percent. Here x is energy or PHA channel number. If the distribution is Gaussian, the variance can be obtained from the FWHM using the relation

$$\sigma_x = \frac{FWHM_x}{2.354} \quad .$$

Thus,

$$V = 0.1805 \; R^2 \quad .$$

A. Photomultiplier Tubes

1. Variance. The variance of the pulse height distribution produced by a photomultiplier tube illuminated by constant amplitude light pulses is a result of statistical fluctuations in the number of photoelectrons produced and statistical fluctuations in the multiplication by the dynodes. Assume that a light pulse deposits N photons on the photocathode of a PMT. A fraction ε_q, the quantum efficiency, of these photons will eject photoelectrons. A fraction ε_d of these photoelectrons will be collected at the first dynode. Then $n = N\varepsilon_q\varepsilon_d$ is the number of photoelectrons collected at the first dynode. Since ε_q and ε_d represent Bernoulli trials, n will have a Poisson distribution if N does. The variance will then be $V_n = 1/\bar{n}$, where $\bar{n} = N\bar{\varepsilon}_\phi\bar{\varepsilon}_d$ (the bar represents average values). The variance in the output pulses, called the statistical variance V_s, is given by

$$V_s = \frac{1 + V_m}{\bar{n}} \quad ,$$

where the multiplication variance V_m accounts for statistical fluctuations in the multiplication at the dynodes. V_m has been calculated for a few idealized cases. If the multiplication at the dynodes is described as a Poisson distribution (an assumption found to be overly optimistic for most PMT's), then

$$V_m \simeq \frac{1}{\delta - 1} \quad ,$$

where δ is the multiplication at the first dynode. If single photoelectron events produce an exponential pulse height distribution, then $V_m = 1$. Measurements of V_m have ranged from 0.4 to 1 (Breitenberger [1] Swank and Buck [2], Prescott and Takhar [3]).

2. <u>Gain.</u> At normal operating voltages, the gain δ of a single dynode varies with interdynode voltage approximately as $V^{0.7}$. In a PMT with k stages, with equal voltage per stage, the tube gain varies approximately as $V^{0.7k}$. Since PMT's may have up to 13 stages, the output is very sensitive to high voltage, and voltage stability is important to maintain good resolution.

3. <u>Linearity.</u> At high anode currents, PMT output becomes non-linear due to space-charge effects, usually strongest between the last two dynodes. An idealized derivation predicts that the limiting current density I between two electrodes is

$$I = \frac{2.34 \ V^{3/2}}{d^2} \ \mu A/cm^2 \quad ,$$

where d is the distance in centimeters between the electrodes and V is the potential difference in volts (Parsons [4]). Space-charge effects generally become significant at approximately 1 to 10 mA anode current. This value refers to pulsed current and is typically significantly larger than the allowable continuous current. Space-charge effects can be minimized by distributing the high voltage so that a relatively large potential difference appears across the last two dynodes.

Nonlinearity may also be present at high count rates if the dynode voltages are supplied by a resistor bleeder string. As current through the PMT increases, the voltages at the dynodes change. The redistribution of voltage results at first in an increase in gain. At very high rates, the required current cannot be supplied and the gain drops. This nonlinearity has been examined analytically by Lush [5] and Land [6]. As

a rule of thumb, resistor bleeder string current should be at least ten times the average anode current. Capacitors placed across the last several dynodes can maintain linearity during individual large pulses or short bursts of pulses. Other techniques include using Zener diodes or transistors in the bleeder string and active control of the high voltage (Kovash and Blatt [7], Kerns [8], Hiebert, et al. [9]).

Other causes of nonlinearity are cathode resistivity and fatigue at high light intensities (Keene [10]). These effects are negligible for most scintillation detector applications.

B. Sodium Iodide Scintillators

1. Luminous Efficiency. The luminous efficiency of a scintillator may be expressed as the ratio of light energy produced to ionization energy deposited or as the number of optical photons produced per unit ionization energy loss. Estimates of NaI luminous efficiency have ranged from 20 photons/keV to 50 photons/keV (Lindow, et al. [11], Bellian and Dayton [12]; Akimov [13], Knoll [14]).

2. Linearity. It has been found that scintillation light output is not proportional to ionization energy loss in sodium iodide scintillators. Figure 1 shows light intensity per unit energy deposited as a function of gamma-ray energy (Zerby, et al. [15]). The curve was determined by a Monte-Carlo calculation. The points represent their measurements and can be seen to fit the predictions well. The output is approximately 15 percent high at energies between 10 keV and 100 keV, relative to output at 662 keV.

3. Intrinsic Line Width. The nonlinearity of sodium iodide introduces an additional source of variance. A primary gamma ray can produce secondary electrons in NaI in any number of ways, depending on the number of Compton scatters and the energy deposited per scatter. Each distribution of secondary electrons results in a different average light output due to the nonlinearity of the NaI. Thus, the distribution of light output for a monoenergetic beam of gamma rays is wider than a Poisson distribution of photons. The intrinsic line width V_I is defined by

$$V_I = V_x - \frac{1}{\bar{x}} \quad ,$$

where V_x is the total variance in the distribution of the number x of photons produced. For a Poisson distribution, $V_x = 1/\bar{x}$ and $V_I = 0$. Thus, ordinary statistical fluctuations in x are not included in the definition of intrinsic line width. V_I has been calculated by Iredale [16], Zerby, et al. [15], and Narayan and Prescott [17]. The Monte-Carlo

4
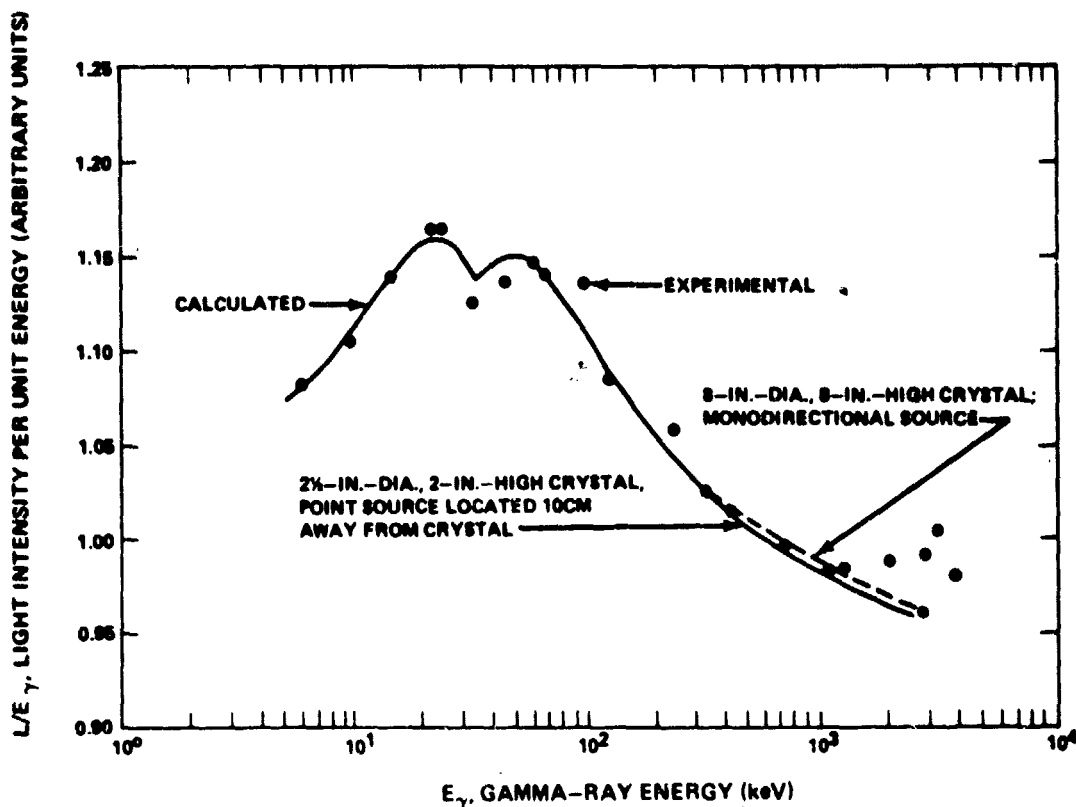
Figure 1. Nonlinearity of NaI (Tℓ) output as a function of
gamma-ray energy, from Zerby et al. [15]. The
vertical axis is normalized to 1 at 662 keV.

calculations of Narayan and Prescott [17] are shown in Figure 2, where
V_I is plotted as a function of the energy of the incident photon. V_I is
small at low energies, where photoelectric absorption dominates, and rises
to a maximum at approximately 500 keV, where one or more Compton
scatters are likely. At still higher energies, V_I drops due to the averag-
ing effect of many Compton scatters. The step at 33 keV is due to the
K edge of iodine.

C. Transfer Variance and Light Collector Housings

The probability that an optical photon emitted by the scintillator
will result in a photoelectron collected at the first dynode of a PMT is
called the transfer efficiency T. T can be expressed as

$$T = \epsilon_L \epsilon_q \epsilon_d \quad ,$$

5

ENERGY (keV)
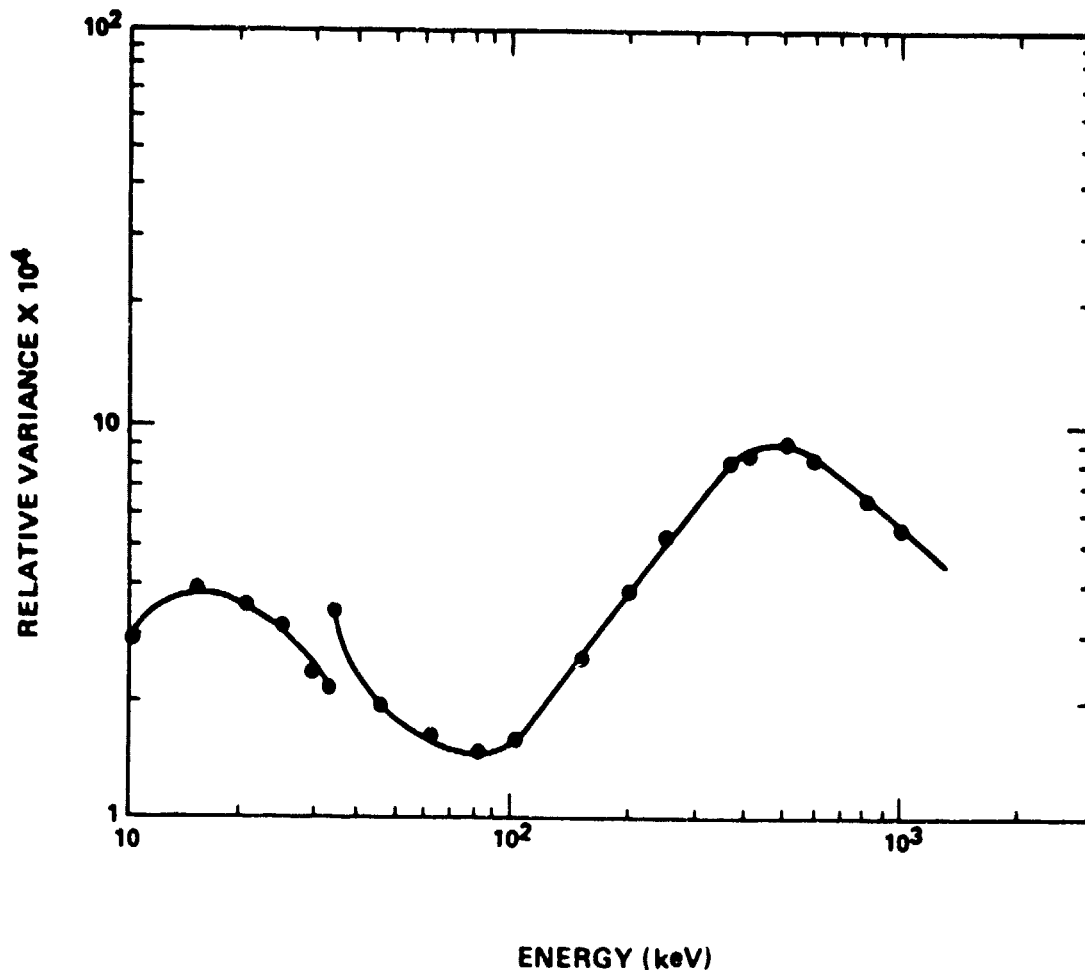
Figure 2.   Intrinsic line width of NaI (Tℓ) due to nonlinearity,
as calculated by Narayan and Prescott [17].

where ϵ_L is the efficiency for collecting light at the photocathode, ϵ_q is the quantum efficiency of the photocathode, and ϵ_d is the efficiency for collecting photoelectrons at the first dynode.

The transfer efficiency will probably depend on the location within the crystal at which a photon is emitted. The variance in the distribution of transfer efficiencies is called the transfer variance V_T.

Large scintillators require some type of light collector housing or light pipes to bring the light to the photomultiplier tube. The design of the light collectors attempts to satisfy two requirements:

1)   The efficiency of light collection must be high to keep the statistical variance low.

6

2) The uniformity of light collection must be high to keep the transfer variance low.

These two goals can conflict in the geometrical design of a light collector housing.

Clay and Gregory [18] have studied light collection from a 1 m^2 plastic scintillator onto a single photomultiplier tube. They found that a number of white paints are satisfactory for the reflecting surfaces inside the housing and that uniformity improves with increasing distance between scintillator and PMT. The uniformity can be improved by placing a reflecting disc midway between the scintillator and the PMT to block some of the light that would fall directly on the PMT, but this procedure reduces the pulse height somewhat.

D. Resolution of a Detector System

The various sources of variance in a sodium iodide detector system can be combined to yield an output pulse variance V_o for monochromatic incident gamma rays [1].

$$V_o = V_T + (1 + V_T) \left(V_x - \frac{1}{\bar{x}} \right) + \frac{(1 + V_m)}{\bar{x} \, \bar{T}} \qquad :$$

where

$\bar{x}$ = average number of photons produced

V_x = variance in number of photons produced

$\bar{T}$ = average transfer efficiency

V_T = variance in T (transfer variance)

V_m = variance in multiplication of PMT

$\bar{x}\bar{T}$ = number of photoelectrons collected at first dynode.

Since V_T is usually much less than 1, the formula may be approximated as

$$V_o = V_T + V_I + V_s \quad .$$

where V_T is the transfer variance, $V_I = V_x - \dfrac{1}{\bar{x}}$ is the intrinsic line width, and $V_s = (1 + V_m)/(\bar{x} \; \bar{T})$ is the statistical variance.

III. PROCEDURES

This section describes the test procedures in sufficient detail to enable the reader to duplicate the tests. This section also provides the information necessary to judge the validity and accuracy of the results presented in the next section.

A. Photomultiplier Tube Tests

The photomultiplier tubes tested were EMI type D302B, which are 11-stage tubes with 12.7 cm (5 in.) diameter bialkali photocathodes. Also tested was an EMI type 9709R which has nine stages and an S11 photocathode. The dynode resistor bleeder string used is shown in Figure 3. The resistances are those recommended by EMI for very high pulsed current NaI(Tl) application. A relatively large resistance is used between the last two dynodes to reduce space-charge limiting of large pulses. EMI recommends that the resistor between the cathode and first dynode be selected to provide a potential difference of 450 V. We used 3.9 MΩ for this resistance and tested other values. The tubes were enclosed in magnetic shields for all of the tests.

Photomultiplier outputs were fed into an Ortec Model 113 preamplifier set at 0 pF input capacitance. Preamp pulses were fed into a TC 203BLR spectroscopy amplifier with $\tau = 1$ μs, BLR = out. The monopolar ac inverted output was fed into a Tracor Northern 1710 pulse height analyzer. The fine gain of the amplifier was set at 1.0, allowing direct comparison of pulse heights obtained at different coarse gains. A block diagram of the experimental setup is shown in Figure 4.

PMT performance was tested using a green light-emitting diode (LED) covered by a translucent diffuser. Pulses were supplied by a BNC BH 1 tail pulse generator. The rise time was 0.5 μs and the fall time was 1.0 μs. The tail pulse generator was triggered by the 1 kc calibration pulse from a Tektronix 454 oscilloscope to ensure reproducibility. The tail pulse generator was also used to gate the PHA, thereby greatly reducing noise and allowing the lower level discriminator on the PHA to be set to zero. The distance between the LED and the photocathode is not critical but should be large enough to ensure fairly uniform illumination of the photocathode (several inches). The LED electronic setup is also shown in Figure 4.

8

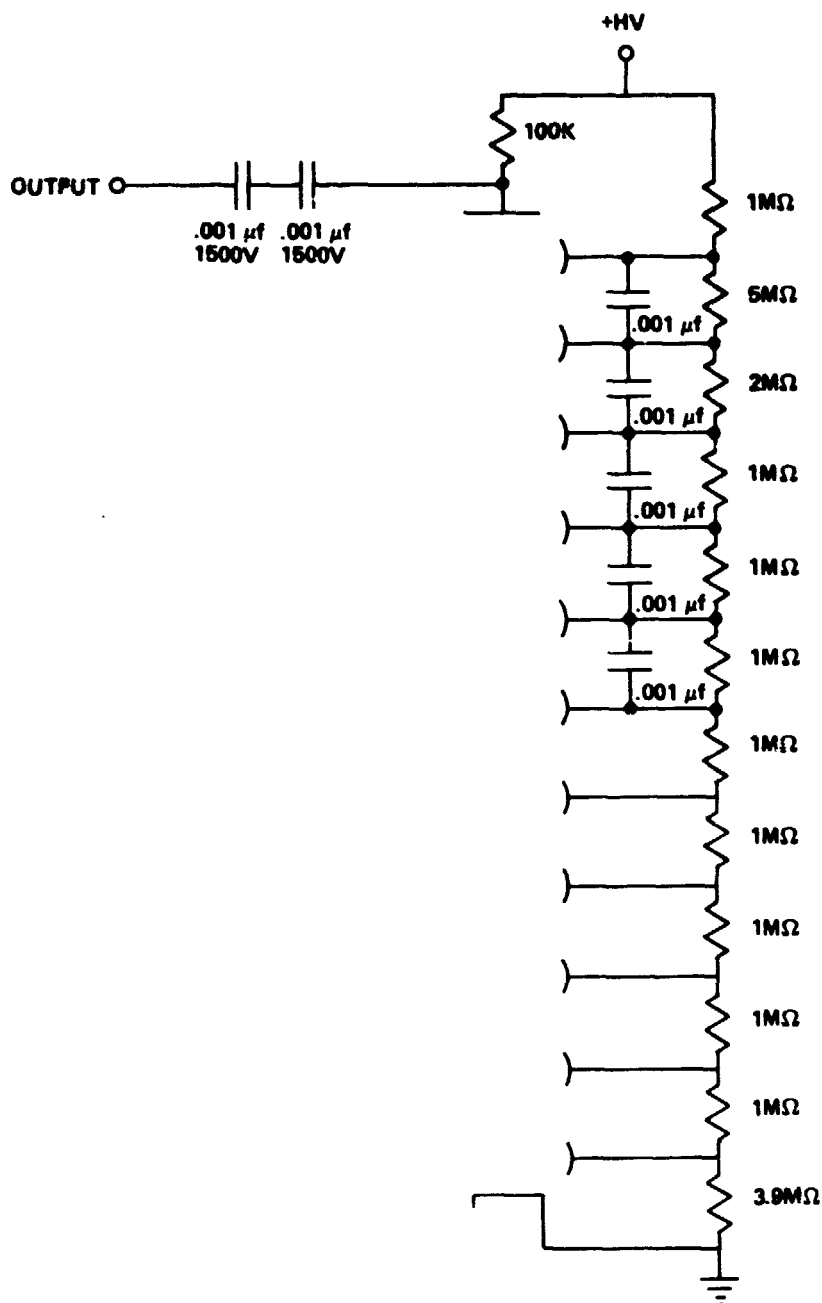Figure 5. Resistor bleeder string used on 11-stage EMI
Type D302B photomultiplier tubes.

It is important to recognize that LED light output cannot be expected to be independent of pulse rate, since output is temperature dependent, nor is light output proportional to input pulse voltage. However, the number of photons emitted does appear to be Poisson distributed for constant input pulse heights.
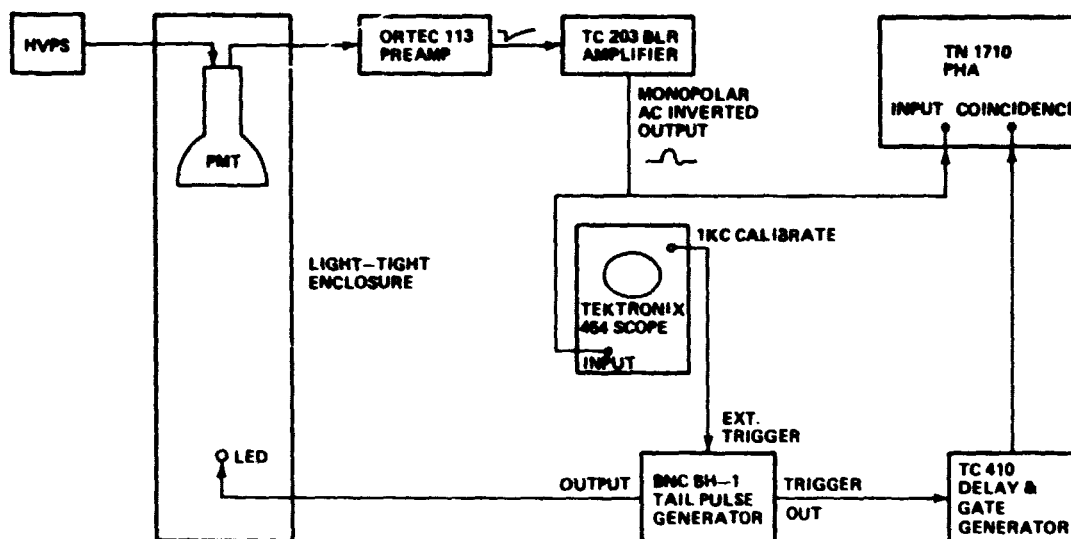
Figure 4. Setup for testing photomultiplier tubes with
LED pulses.

1. **Single Photoelectron Response.** The LED can be used to determine the response of the PMT to single photoelectrons. From this information, pulse heights can be converted to number of photoelectrons and V_m can be measured. The procedure, in general outline, is as follows:

1) Determine noise spectrum with LED off.

2) Turn LED to an amplitude such that pulses are occasionally seen.

3) Subtract noise spectrum, corrected for deadtime.

4) Compute x_1, the average channel number for single photoelectrons, correcting for events in which more than one photoelectron was obtained.

A detailed description of the procedure is given in the Appendix.

2. **Multiplication Variance.** Once a conversion between pulse height and number of photoelectrons is obtained, the PMT multiplication variance V_m can be determined by measuring the variance of the pulse height distribution as a function of number of photoelectrons. Details of the procedure are given in the Appendix. V_m should be measured at several different LED intensities. At high intensities, space-charge limiting may reveal itself as an apparent decrease in V_m.

The measurement of x_1 need be made at only one value of high voltage. To determine x_1 as a function of voltage, simply find relative PMT gain as a function of high voltage using a constant amplitude LED

10

pulse. To ensure that space-charge limiting does not occur at the higher voltages, verify that the relative variance at fixed LED amplitude does not drop with increasing voltage. At low voltages (approximately 600 V) the variance increases sharply due to poor collection of the photoelectrons.

Note that even if x_1 and V_m are not accurately determined, the measured variance is still a valid measurement of the statistical variance V_s versus pulse height. When the scintillation crystals are tested, the contribution of V_s to the total relative variance is, therefore, known quite accurately.

3. Space-Charge Limiting. Nonlinearity due to space-charge effects was measured using several techniques. Several difficulties are involved in making such measurements. One difficulty is that we are interested in nonlinearity of pulses, not the dc current levels often used in investigations of nonlinearity. With pulses from sodium iodide, the PMT anode current rises rapidly to a peak value and then decays exponentially with a 0.25 μs time constant. The peak of the pulse will exhibit saturation before the exponential tail, as can be seen easily with an oscilloscope. Consequently, the pulse height nonlinearity depends on the timing characteristics of the output circuitry and the integration time of the amplifier. A fast peak-and-hold technique will exhibit greater nonlinearity than integration of the pulse over several time constants. Another difficulty is specification of the independent variable to avoid confusion. Traditionally, anode current is the independent variable, but this is precisely the quantity that saturates. We use "expected peak anode current", defined as the anode current, at the peak of the pulse, that would be expected in the absence of saturation effects.

The advantage of using anode current as the independent variable is that the nonlinearity curves will not vary much from tube to tube nor show a high dependence on tube gain, although there is a dependence on voltage at the saturating stage. The anode current is measured by feeding the output of the PMT to a 50 Ω termination instead of the preamp. Since the RC time constant of the output circuit is so short (a few nanoseconds), the voltage across the terminator tracks the anode current reasonably accurately. Therefore, the peak anode current equals the peak voltage across the terminator, measured from an oscilloscope, divided by termination resistance.

Three different procedures were used to measure PMT nonlinearity. In the first, an LED and a single optical filter were used. The LED was pulsed using a tail pulse generator with the rise and fall times set to match the pulse shape from NaI as closely as possible. The transmission of the filter was obtained by measurements at low LED intensities. The PMT output was determined with and without the filter for a wide range of LED intensities. Figure 5 shows the experimental configuration. A difficulty with this procedure is that at high light intensities the anode current shows saturation effects even with the filter in place. Therefore, the linearity curve must be built up a step at a time, starting at low light intensities. It should be noted that LED nonlinearity precludes meaningful comparisons of pulse heights obtained at different input pulse amplitudes.
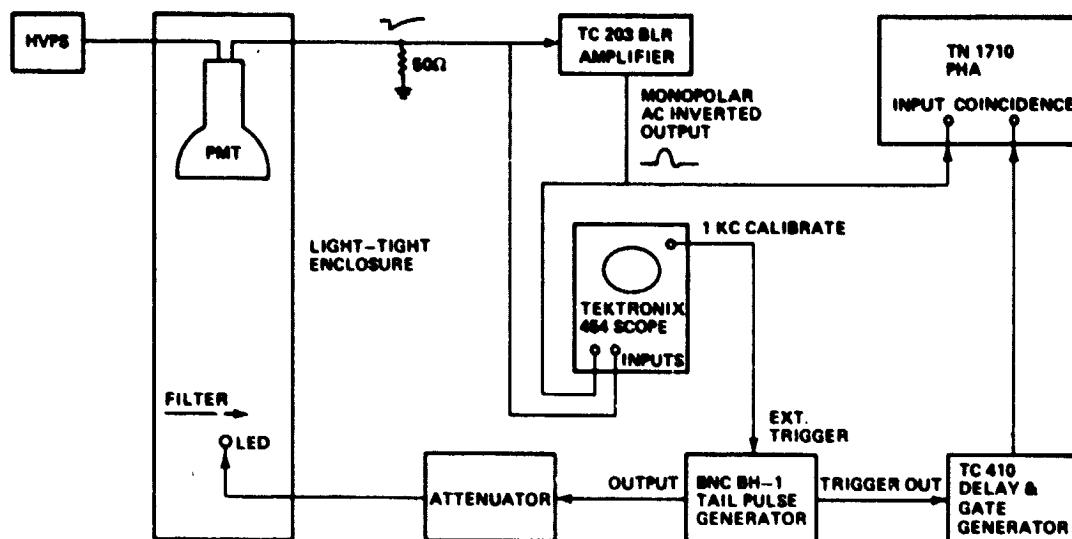
11

Figure 5. Setup for testing photomultiplier linearity at
large pulse amplitudes.

The second method is similar to the first except that the LED is
set at its highest intensity and a series of Wratten filters ranging from
ND 0.5 to ND 4 are interposed. This procedure is faster than the first
but requires accurate knowledge of the filter densities. Care must be
taken that no light can leak around the filter to the PMT.

The third method employs radioactive sources and NaI crystals to
produce the light pulses. The ratio of the pulse heights produced by
two radioactive sources is determined as a function of PMT high voltage.
The ratio of the light input to the PMT is not necessarily the ratio of
the gamma-ray energies, since NaI output is not linear with energy
deposited. The input ratio is determined by measurements at low values
of PMT high voltage. With this procedure, the linearity curve does not
apply to any single value of high voltage. However, the gain of an
11-stage tube is so strongly dependent on voltage that the entire linearity
curve can be produced with a variation of approximately 300 V. Advan-
tages of this technique are that there is no question about the pulse
shape accurately matching that of sodium iodide and that the nonlinearity
can be determined at particular values of gamma-ray energy for the
specific detector system being tested.

4. High-Rate Effects. The gain of a PMT using a resistive dynode
bleeder string depends on count rate, as described in Section II.A. This
effect cannot be tested reliably with an LED, since LED light intensity is
not necessarily independent of pulse rate. Instead, the PMT was coupled
to a 12.7 by 1.27 cm (5 by 0.5 in.) NaI crystal illuminated by 60 keV
gamma rays from a 10 mCi Am^{241} source. The PMT output was fed to a
50 Ω termination resistor. Average anode current I_a was determined from
the equation

12

$$I_a = \frac{V\tau r}{R} \quad ,$$

where V is the peak voltage across the 50 Ω resistor when a 60 keV gamma ray is detected, $\tau = 0.24$ μs is the NaI scintillation decay time, r is the count rate, and R = 50 Ω. This equation may be understood in the following way: V/R is the peak anode current; Vτ/R is the integrated current during a pulse, or the charge transferred in one pulse; I_a, the average

rate of charge flow, is then (Vτ/R) r. The rate r is varied by varying

the distance between the Am^{241} source and the crystal. The 60 keV pulse height is then measured as a function of count rate. The average anode current is measured only once, at low count rate. The expected average anode current is then scaled as the count rate. The actual average anode current is just the expected average anode current times the fractional change in pulse height. It is useful to compare average anode current to the bleeder string current at zero count rate. With high voltage set at 1600 V, the quiescent bleeder string current is 80 μA.

     5. Other Tests. PMT gain and resolution were determined as a function of high voltage using LED pulses. Resolution was investigated as a function of cathode to first dynode voltage by changing the appropriate resistor in the bleeder string. PMT noise rate was measured as a function of time since exposure to room lights.

     B.   12.7 by 1.27 cm (5 by 0.5 in.) NaI(Tℓ) Crystal

     After determining the conversion between pulse height and number of photoelectrons and determining V_m for a photomultiplier tube, additional sources of variance in a NaI(Tℓ) detector system were investigated. A Harshaw 12.7 by 1.27 cm (5 by 0.5 in.) NaI(Tℓ) crystal with a reflecting rear surface was coupled to a 12.7 cm (5 in.) photomultiplier tube using Dow Corning optical coupling compound. Gamma-ray sources of known energy were used to determine pulse height (and thus $\bar{n}_{pe}$) and total variance as a function of energy deposited in the crystal. Tests were made with uniform illumination of the crystal by the gamma rays and with the gamma rays collimated by a lead absorber to a small region in the center of the crystal. The difference in resolution between collimated and uncollimated beams provides an estimate of the transfer variance in the uncollimated case.

     The gamma-ray sources used and the energies emitted are given in Table 1. Co^{57} was not used because this isotope emits gamma-ray lines at 122 keV and 136 keV, resulting in a single anomalously broad line at approximately 124 keV. Many detector manufacturers specify resolution at the 662 keV line of Cs^{137}. As will be shown in Section IV, however, the variance at 662 keV is dominated by NaI intrinsic line width. Therefore, resolution at this energy does not provide a sensitive indicator of

TABLE 1. GAMMA-RAY SOURCES

Source	Energy (keV)	
Mo K X-ray	17.4	
Ag K X-ray	22.1	
Ba K X-ray	32.2	Variable Energy X-ray Source
Tb K X-ray	44.5	
Am^{241}	59.5	
Cd^{109}	22.1	
	88	
Ba^{133}	30.6	
	81	
	356	
Na^{22}	511	
	1275	
Cs^{137}	662	
Mn^{54}	835	

light collection efficiency or uniformity. In using sources emitting gamma rays of more than one energy, the lower energy peaks may be distorted due to background from lines of higher energy. Background spectra were subtracted from source spectra before deter...ining the peak and width of gamma-ray lines.

C. Light Collector Housings and 50.8 by 1.27 cm (20 by 0.5 in.) NaI(Tℓ) Scintillation Crystals

A number of tests were made to determine the characteristics of detectors using 50.8 by 1.27 cm (20 by 0.5 in.) crystals viewed by three PMT's. The main goals of these tests were to determine the light emission efficiency and uniformity of several types of crystals and to determine the optimum geometry for the light collection housing. Figure 6 illustrates the geometry of the detector system. The crystals are viewed by three photomultiplier tubes on a circular plate. A cone or cylinder supports the PMT plate above the crystal. The interior surfaces of the cone and PMT plate were painted with Eastman No. 6080 white reflective coating, applied approximately 1 mm thick in accordance with the manufacturer's recommended procedures.
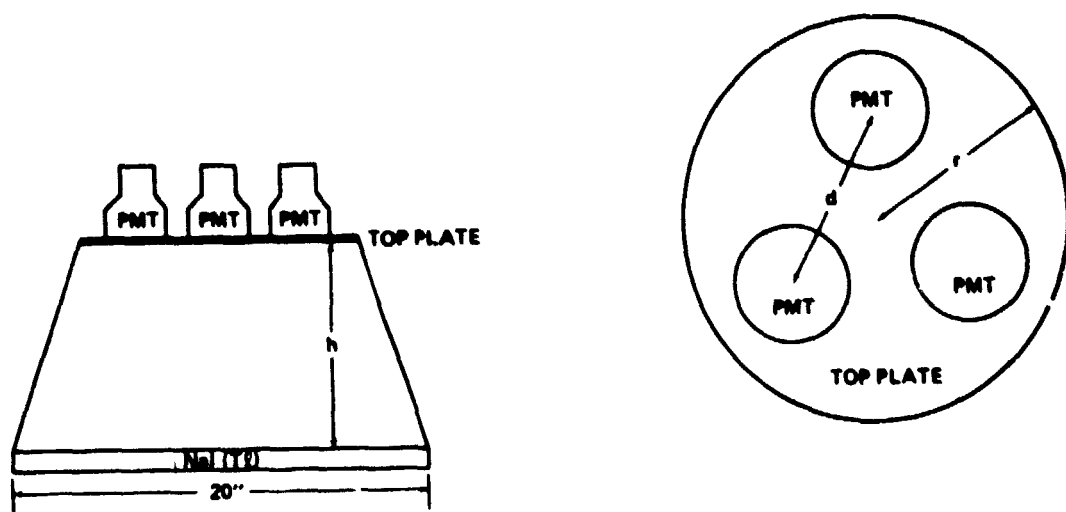
14

Figure 6. Light collection housing mechanical configuration for
testing 50.8 by 1.27 cm (20 by 0.5 in.) NaI(Tℓ) crystals.

The anodes of the three PMT's were summed using a resistance
network. Separate high-voltage power supplies were provided for each
tube and were adjusted to equalize the gains. Figure 7 illustrates the
experimental arrangement. The LED was used to balance tube gains and
to determine the single photoelectron pulse height and multiplication vari-
ance for the summed output using the same procedures as for individual
tubes. Collimated and uncollimated gamma-ray beams were used to investi-
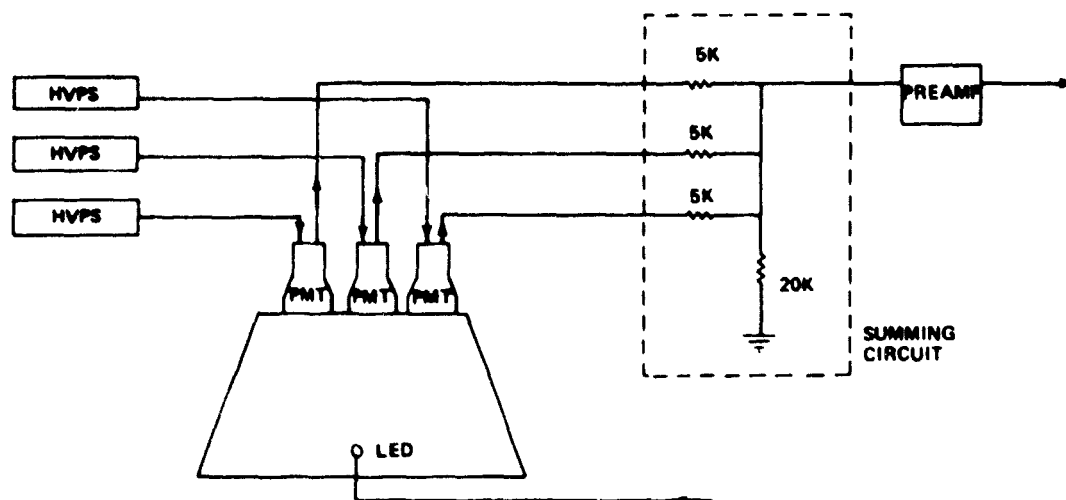gate transfer variance.

Figure 7. Electronic setup for testing 50.8 by 1.27 cm
(20 by 0.5 in.) crystals using three PMT's.

IV. RESULTS

A. Photomultiplier Tube

This section describes the results of tests performed on EMI type D302B photomultiplier tubes. The procedures for some of the tests are described in Section III.A. A few of the tests were performed on three different tubes.

1. <u>Noise.</u> The PMT count rate as a function of time after exposure to room lights was investigated. Figure 8 shows a plot of count rate versus time. The rate decreases rapidly in the first few hours. Subsequently, there is a slow decrease to a minimum, followed by a slow increase. This slow variation is probably due to the change in ambient temperature throughout the night. This test shows that photomultiplier tubes must be kept in darkness at least several hours before performing any tests in which small output pulses must be detected, as in determining the single photoelectron response.

2. <u>Cathode to First Dynode Voltage.</u> EMI recommends that the voltage between the cathode and the first dynode of its 12.7 cm (5 in.) tubes be 450 V. Resolution of an LED pulse of fixed intensity was measured for values of cathode to first dynode voltage V_{K-D1} ranging from 200 to 508 V. The results are shown in Table 2, where V_{K-A} is the cathode to anode voltage. The LED intensity was such that each pulse yielded approximately 55 photoelectrons. The resolution is independent of V_{K-D1}, indicating that this voltage is not critical within the range examined.

3. <u>Single Photoelectron Spectrum.</u> As described in Section III.B, an approximation to the single photoelectron spectrum can be obtained by pulsing the LED at an amplitude low enough that the average number of photoelectrons per pulse is much less than one. Using this procedure, the single photoelectron spectrum for EMI tubes was found. A typical spectrum, shown schematically in Figure 9, is approximately exponential with a flattening at the lowest pulse heights.

4. <u>Multiplication Variance.</u> Multiplication variance V_m is determined by measuring the variance as a function of number of photoelectrons, as described in Section III.B. Since $V_s = (1 + V_m)/\bar{n}_{pe}$, it is customary to plot variance V_s versus $(1/\bar{n}_{pe})$. A straight line of slope $(1 + V_m)$ is expected. Figure 10a shows such a plot. A value $V_m = 0.64$ fits the data well for the three PMT's tested. No variation of V_m with voltage is evident. Figure 10b provides an expanded view of the region of Figure 10a near the origin.
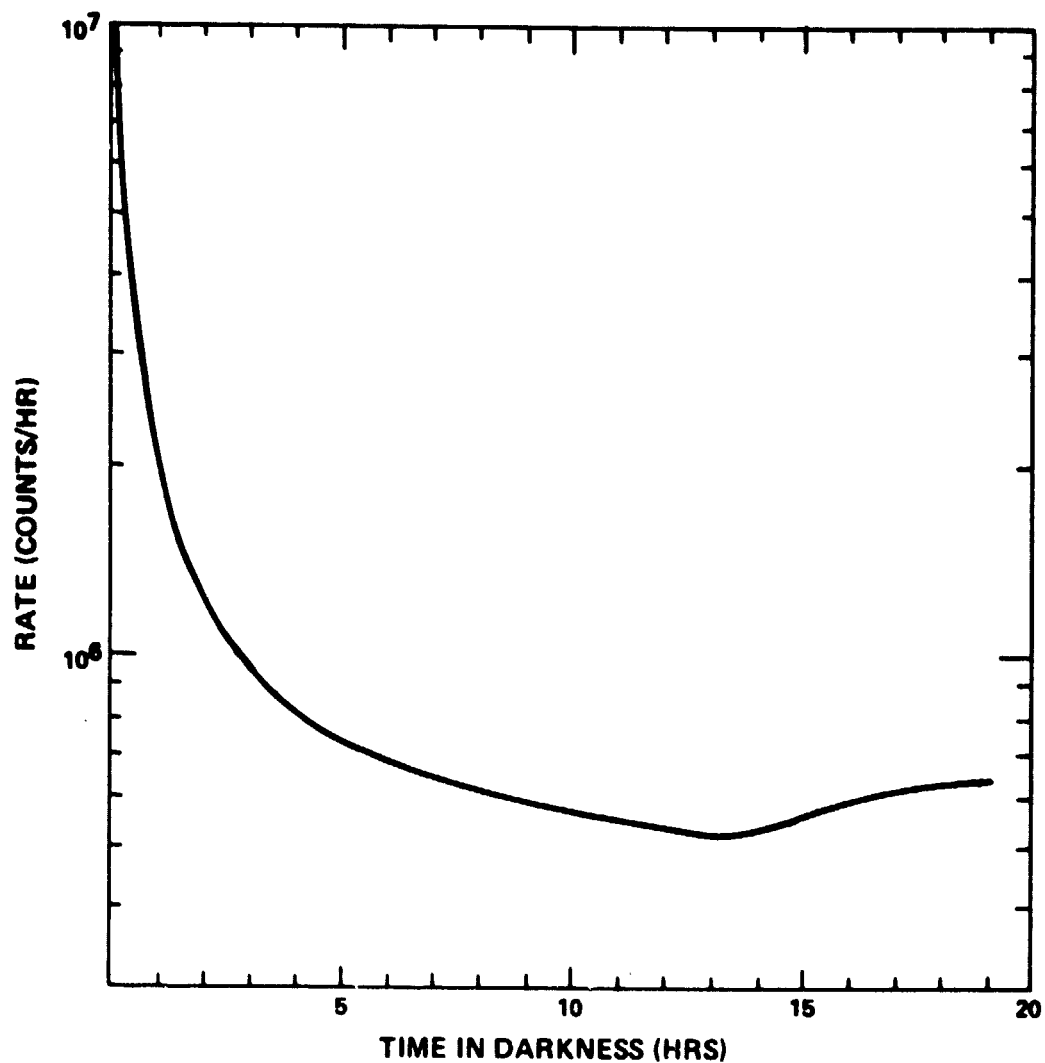
16

Figure 8. Photomultiplier noise rate versus time since exposure to room lights.

TABLE 2. CATHODE TO FIRST DYNODE VOLTAGE

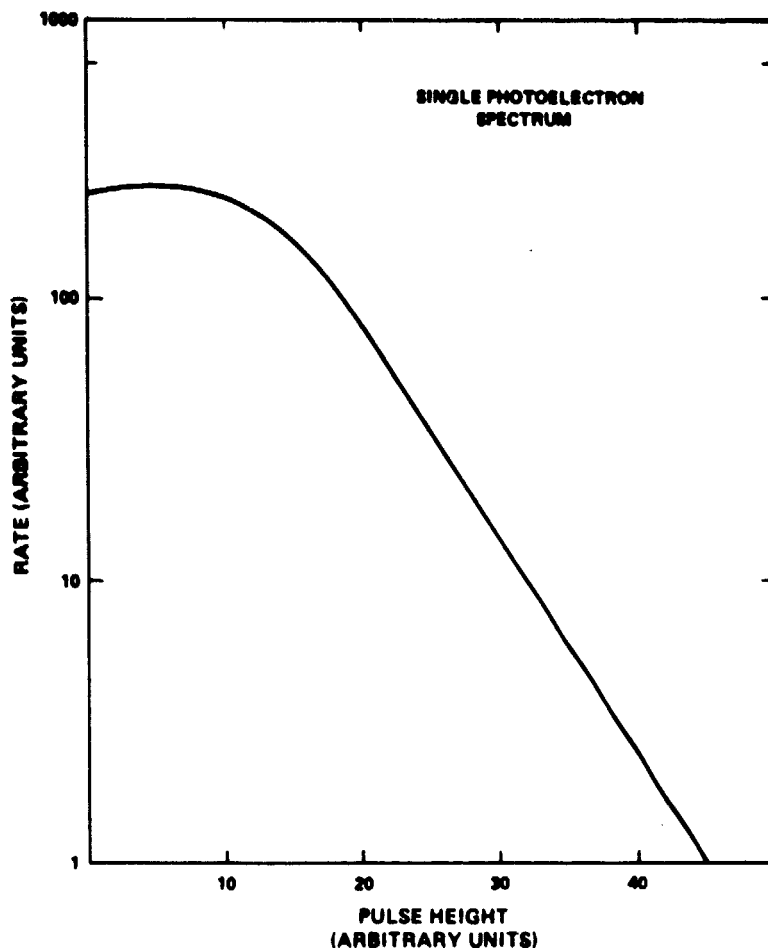| V_{K-D1} (Volts)	V_{K-A} (Volts)	Resolution (FWHM)
200	1000	40%
263	1000	40%
339	1000	39%
508	1600	40%

Figure 9. Idealized shape of single photoelectron spectrum.

5. Gain versus High Voltage. Photomultiplier gain as a function
of high voltage is plotted on a log-log scale in Figure 11 for an 11-stage
and a 9-stage tube. The data are well represented by a straight line.
The slope is 7.6 for tne 11-stage tube and 5.5 for the 9-stage tube.
These values for the slope imply a gain per stage proportional to $(HV)^\gamma$,
where γ = 0.6 to 0.7, about as expected. At higher voltages, the gains
decrease due to space-charge limiting.

6. Space-Charge Limiting. Nonlinearity due to space-charge limit-
ing was measured by the methods described in Section III.A.3. The
results are presented in Figure 12. Nonlinearity, expressed as a percent-
age, is defined as follows:

$$\text{Nonlinearity} = \frac{\text{Expected Pulse Height} - \text{Measured Pulse Height}}{\text{Expected Pulse Height}} \quad .$$

18
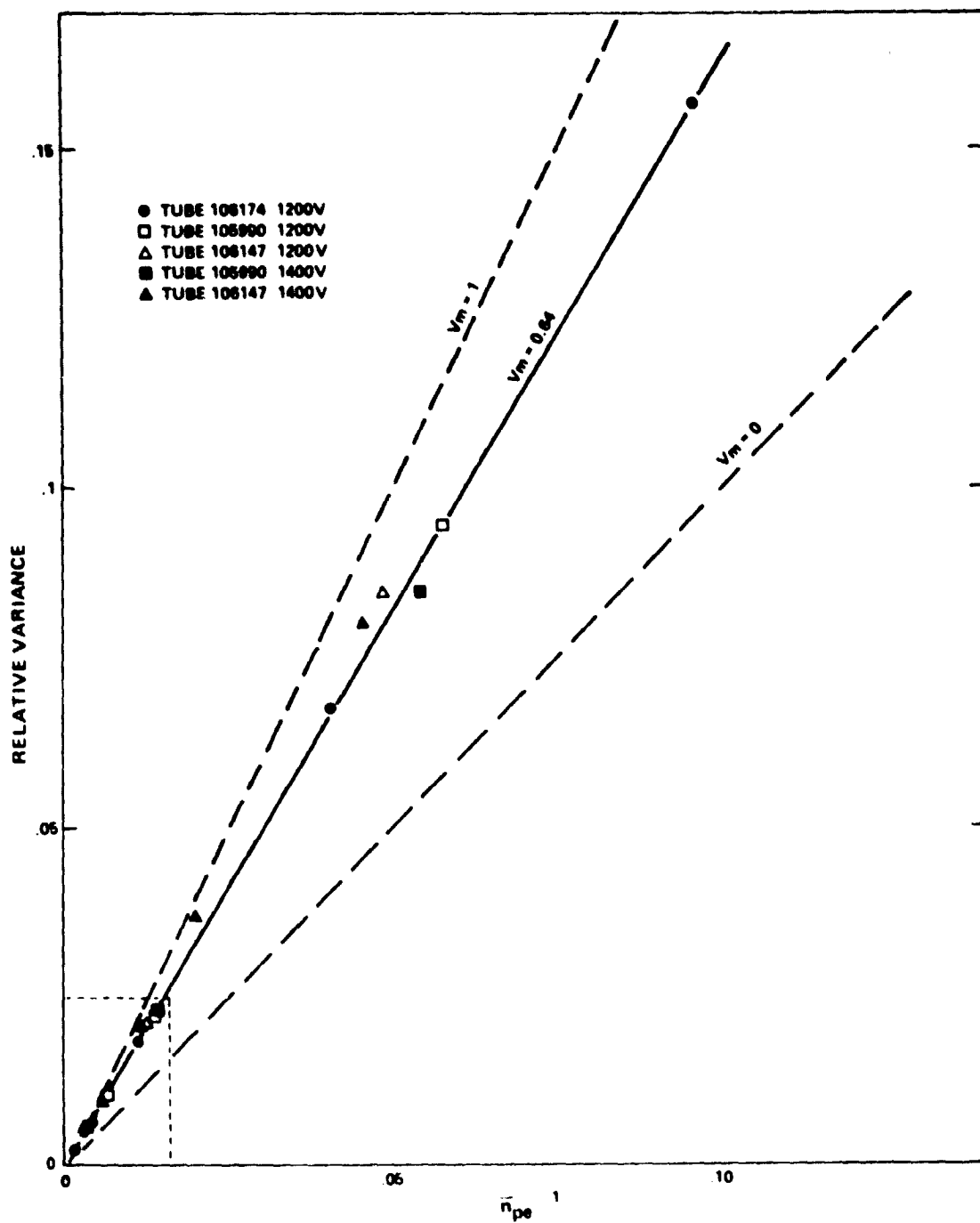
a. Relative variance of PMT output versus $1/\bar{n}_{pe}$. The multiplication variance is approximately 0.64.

Figure 10. Relative variance.
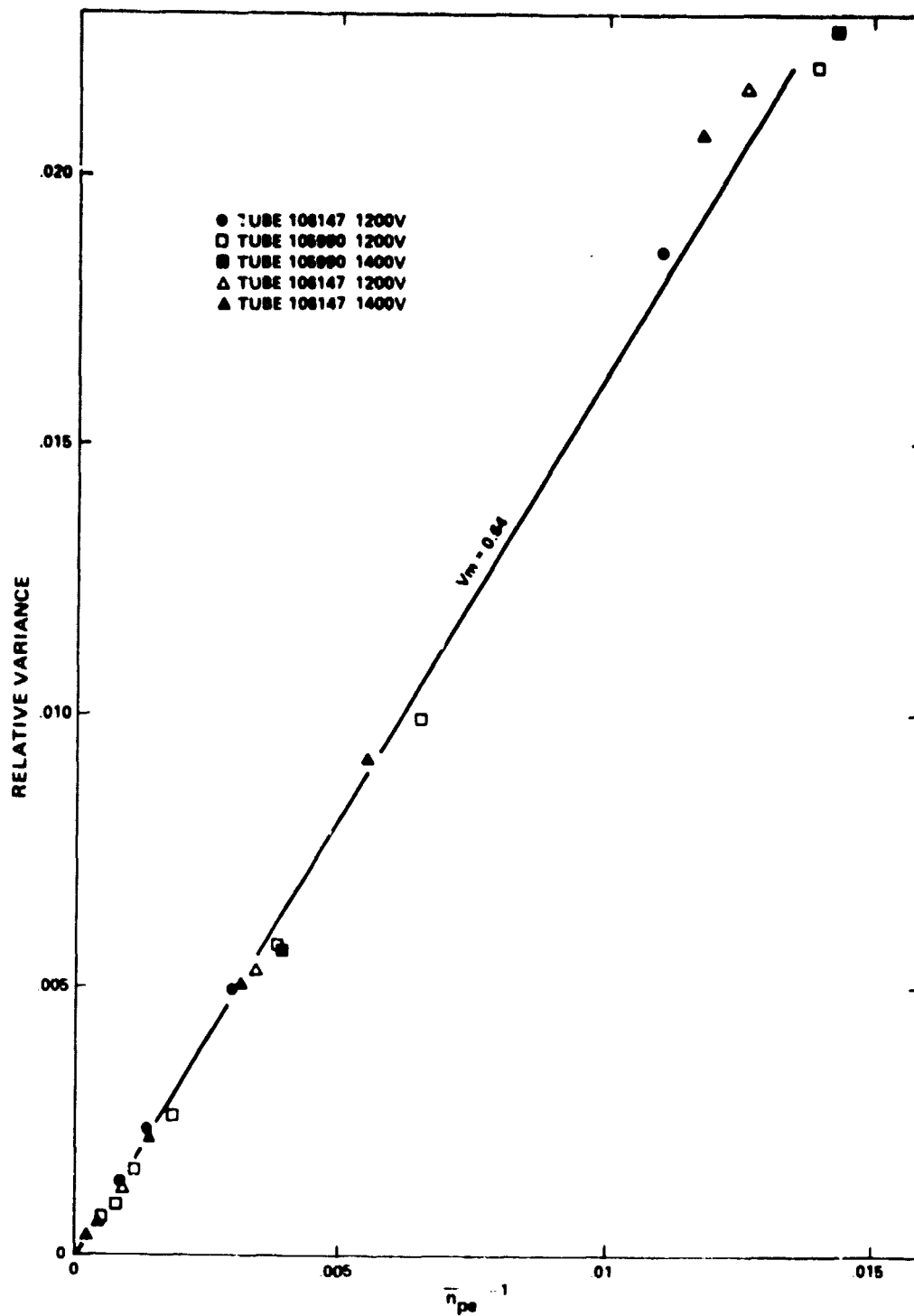
b. Enlargement of region near origin in Fig. 10a.
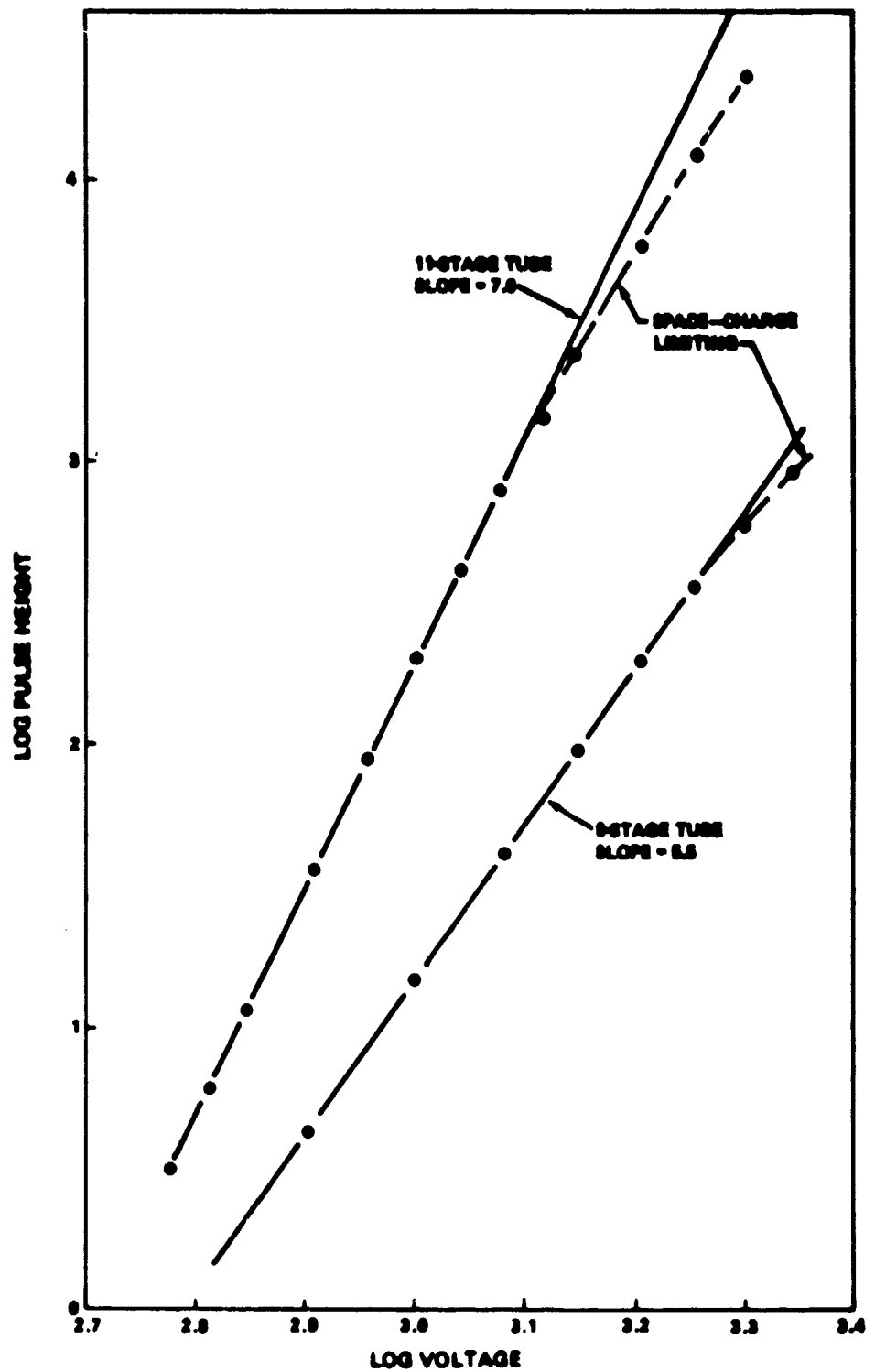
Figure 10. (Concluded).

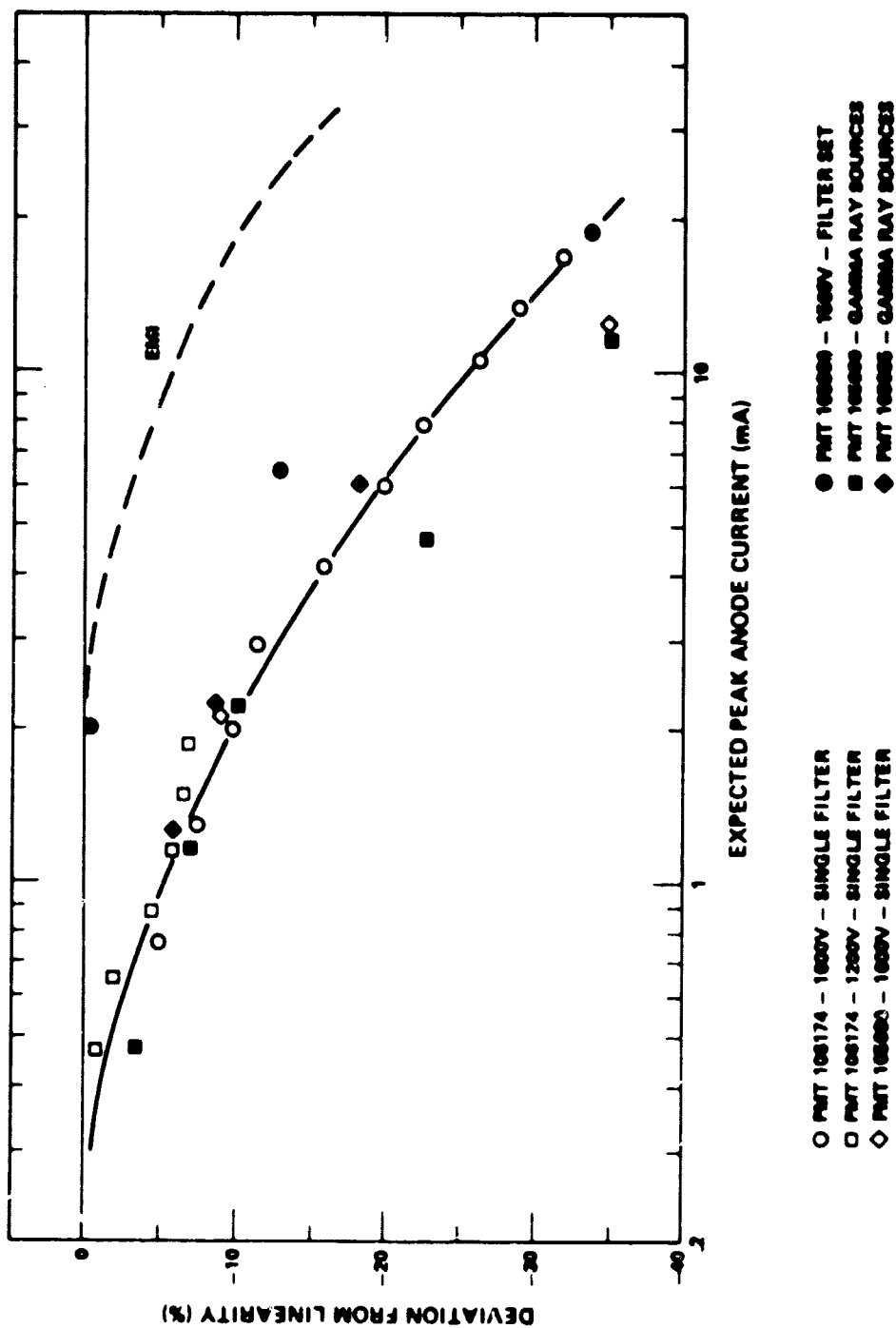Figure 11. Log pulse height versus log high voltage for 11-stage and 9-stage PMT's.

Figure 12. Deviation from linearity due to space-charge effects as a function of expected peak anode current.

22

The expected peak anode current is the peak anode current that would be obtained without space-charge effects. The different symbols represent data taken using various combinations of PMT, high voltage, and technique. The dashed line labeled EMI represents the expected performance presented in the EMI Photomultipliers catalog.

The data indicate that the various techniques agree reasonably well and that the nonlinearity is approximately 5 percent at 1 mA peak anode current and approximately 25 percent at 10 mA peak anode current. The PMT's performed significantly worse than the EMI predictions, which provided no details on the measurement technique.

7. <u>Nonlinearity at High Rates</u>. Nonlinearity occurs at high counting rates as a result of large average current flow causing redistribution of the dynode voltages. Figure 13 shows a plot of measured average anode current I_a as a function of average light intensity, which was varied by changing the distance of an Am^{241} source from the 12.7 by 1.27 cm (5 by 0.5 in.) crystal. The quiescent current through the resistor bleeder string I_b was 80 μA. At low anode currents the measured tube nonlinearity can be well represented by $\Delta Gain/Gain = 0.6 \ (I_a/I_b)$, in reasonable agreement with the calculations of Land [6] and Lush [5]. Therefore, to maintain linearity within 1 percent, the bleeder string current must be 60 times the average anode current. The tube saturates at an anode current of approximately $0.55 \ I_b$.

8. <u>Resolution versus High Voltage</u>. The resolution of the D302B photomultiplier tubes was examined to see if it depended on high voltage. LED pulses yielding about 65 photoelectrons were used. The results are shown in Figure 14. The resolution is approximately constant at approximately 37 percent over the range 700 to 1500 V. At lower voltages, the resolution rapidly degrades, presumably due to poor focusing of photoelectrons. At higher voltages, the resolution appears to improve slightly. This may be due in part to a decrease in V_m and in part to space-charge limiting.

B. Sodium Iodide

1. <u>Luminous Efficiency</u>. Although the luminous efficiency of NaI was not measured directly, a more useful parameter, the number of photoelectrons collected at the first dynode per keV of energy deposited in the crystal, was determined. We call this parameter the system efficiency ε. It may be expressed as $\varepsilon = (\bar{X} \ \bar{T})/E$, where $\bar{X}$ is the average number of photons produced by absorption of a gamma ray of energy E, and $\bar{T}$ is the average transfer variance. Since ε depends on transfer efficiency and gamma-ray energy, the following conditions for its measurement are specified:

1) The energy is 662 keV (Cs^{137} line).

2) The crystal is a Harshaw 12.7 by 1.27 cm (5 by 0.5 in.), directly coupled to the PMT using Dow Corning optical coupling compound.
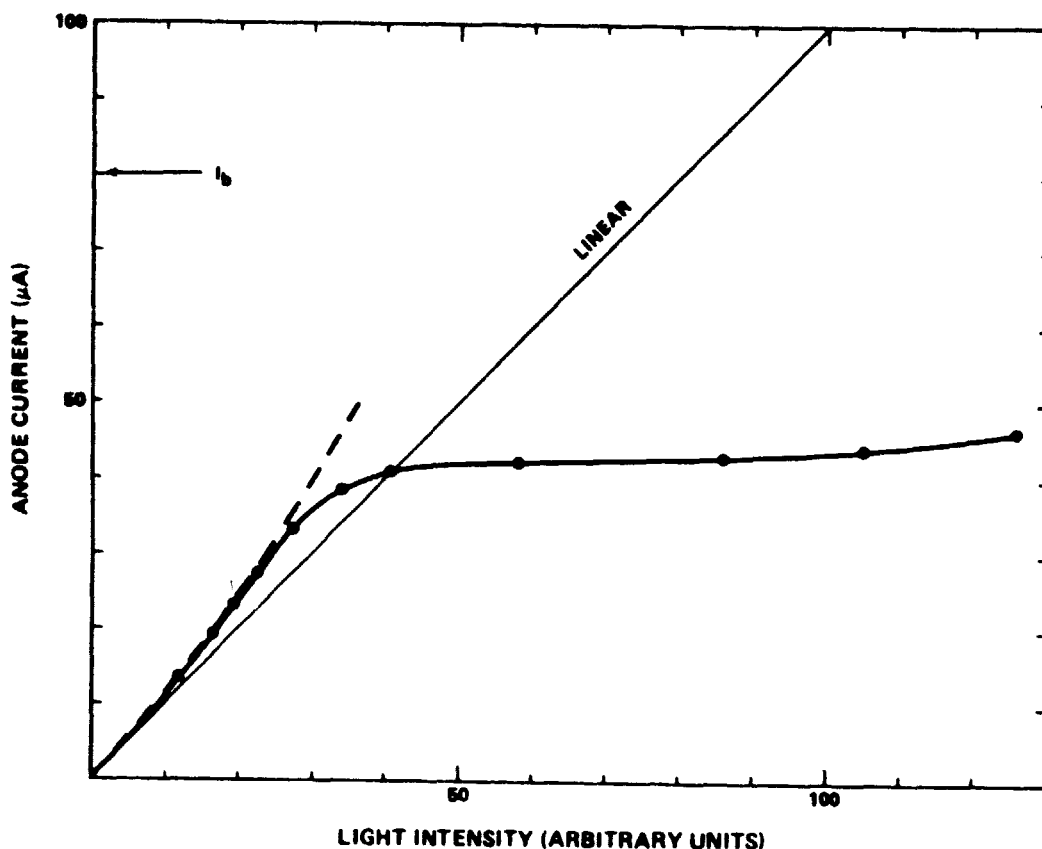
23

Figure 13. Deviation from linearity due to high rates. I_b is the quiescent current through the bleeder string and equals 80 μA. The dashed line represents the relationship ΛGain/Gain $= 0.6 \ I_a/I_b$, where I_a is the anode current.

3) The gamma-ray beam is collimated to a spot at the center of the crystal.

Under these conditions, ε was determined to be 13.9 photoelectrons/keV.

A lower limit to the NaI luminous efficiency is found by assuming perfect light collection ($\varepsilon_L = 1$), perfect photoelectron collection ($\varepsilon_d = 1$), and peak quantum efficiency $_q = 0.27$ for a bialkali photocathode. The luminous efficiency is ≥ 50 photons/keV, which agrees well with the Harshaw specification and corresponds to 15 percent conversion efficiency at 662 keV.

The parameter ε depends upon the measurement of the pulse height for single photoelectrons and thus propagates errors in that measurement. However, a lower limit to ε can be obtained by measuring the resolution at a low energy and attributing all of the variance to photoelectron
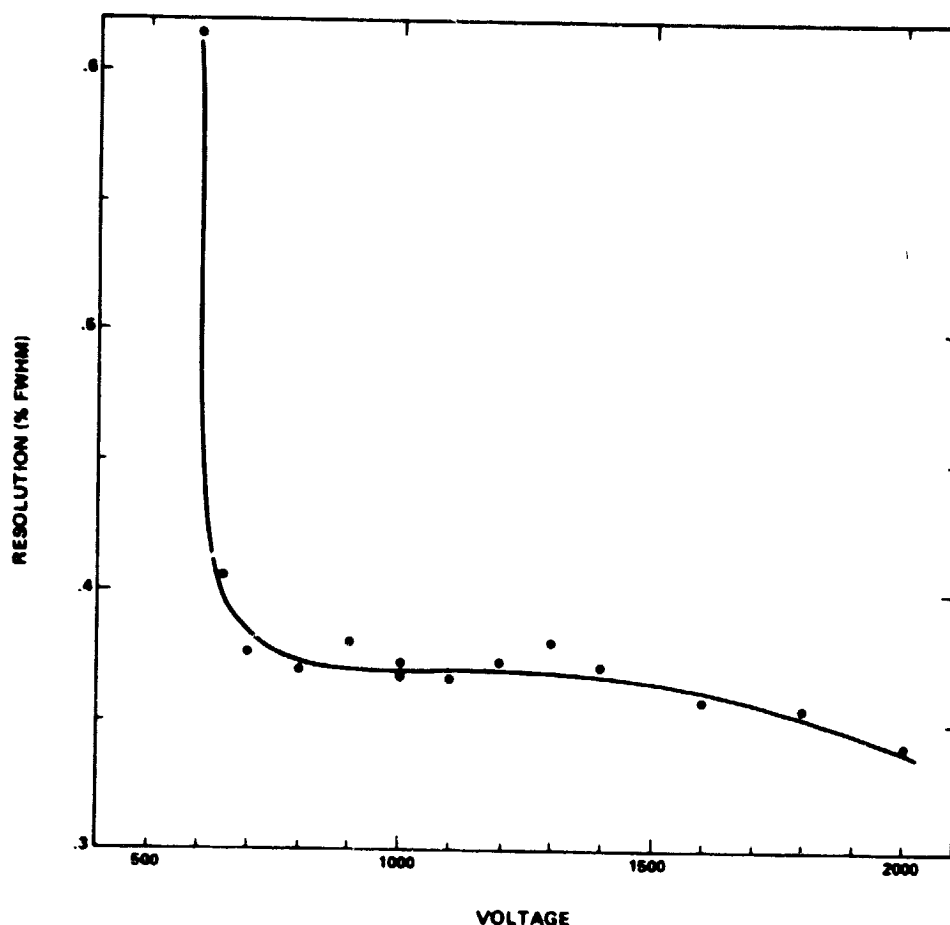
24

Figure 14. Resolution versus high voltage. The large increase below 700 V is probably due to poor collection of photoelectrons. The decrease at voltage greater than 1500 is probably caused by a combination of space-charge limiting and a decrease in V_m.

statistics (i.e., neglect transfer variance and multiplication variance). The resolution at 60 keV (Am^{241}) is 11.8 percent FWHM, indicating $\epsilon > 6.6$ photoelectrons/keV, and luminous efficiency > 24 photons/keV.

2. Nonlinearity. Measurements of pulse height versus gamma-ray energy were made to determine the nonlinearity of NaI(Tℓ) output. The PMT high voltage was low (1000 V) to ensure that space-charge effects were negligible. Figure 15 shows a plot of light intensity per unit energy (normalized to 1 at 662 keV) versus gamma-ray energy. The curve is taken from Zerby, et al. [15]. The solid squares represent our observations using a 12.7 by 1.27 cm (5 by 0.5 in.) Harshaw crystal directly coupled to an EMI 12.7 cm (5 in.) PMT using Dow Corning optical coupling compound. The beam of gamma rays was collimated to an approximately 1 cm spot at the center of the crystal face. Our observations are in excellent agreement with the observations and calculations of Zerby, et al. [15].
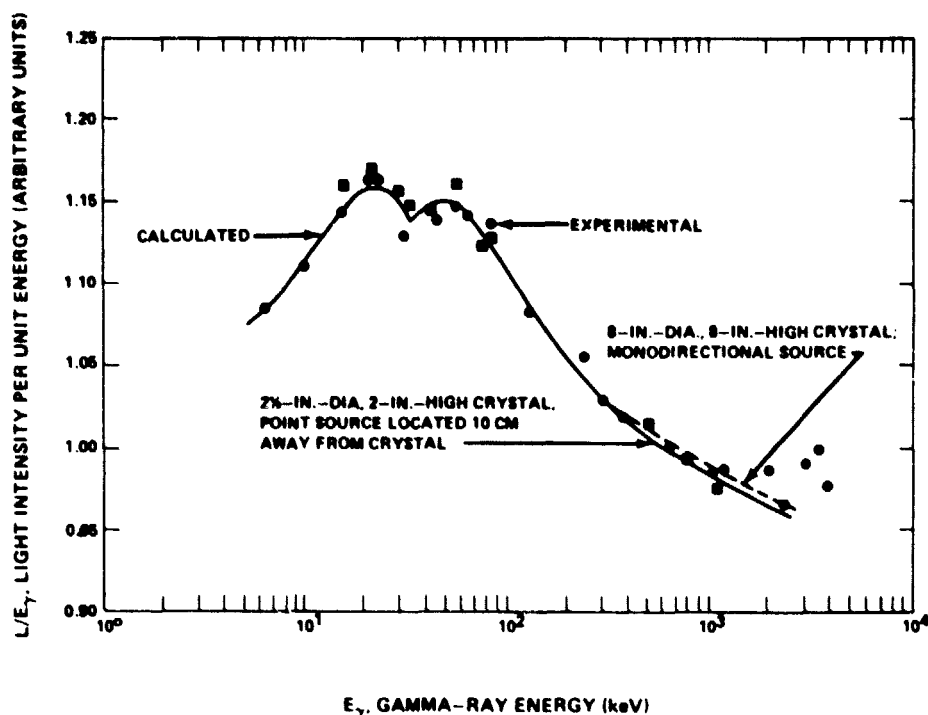
Figure 15. Measured nonlinearity of NaI(Tℓ) output versus gamma-
ray energy. Results obtained here are shown as solid squares
and agree well with calculations and measurements of
Zerby, et al.[15].

3. Variance. Variance of pulse height versus gamma-ray energy
was also determined during the measurements of nonlinearity described
in the last section. The results are plotted in Figure 16. The solid
circles represent data obtained with a collimated beam of gamma rays.
The open circles represent data taken when the gamma sources were
uncollimated and distant enough (∿ 1 m) that the crystal may be consid-
ered to be uniformly illuminated. The solid line represents a calculation
of variance from the equation

$$ V = V_T + (1 + V_T)(V_x \frac{1}{x}) + \frac{1 + V_m}{x\,T} \quad . $$

where the intrinsic line width $[V_x \, (1/x)]$ was taken from Narayan and
Prescott [17], x T (= number of photoelectrons collected) and V_m were
measured, and V_T was set equal to 0. Thus, the curve represents a
minimum variance with no free parameters. The points for the collimated
beam lie slightly above the calculated curve, indicating an additional source
of variance, presumably transfer variance. The discrepancy increases
with decreasing energy. The uncollimated beam results in an additional
transfer variance of approximately 0.002. The ratio of light collection
efficiencies for uncollimated versus collimated beams is 0.95.
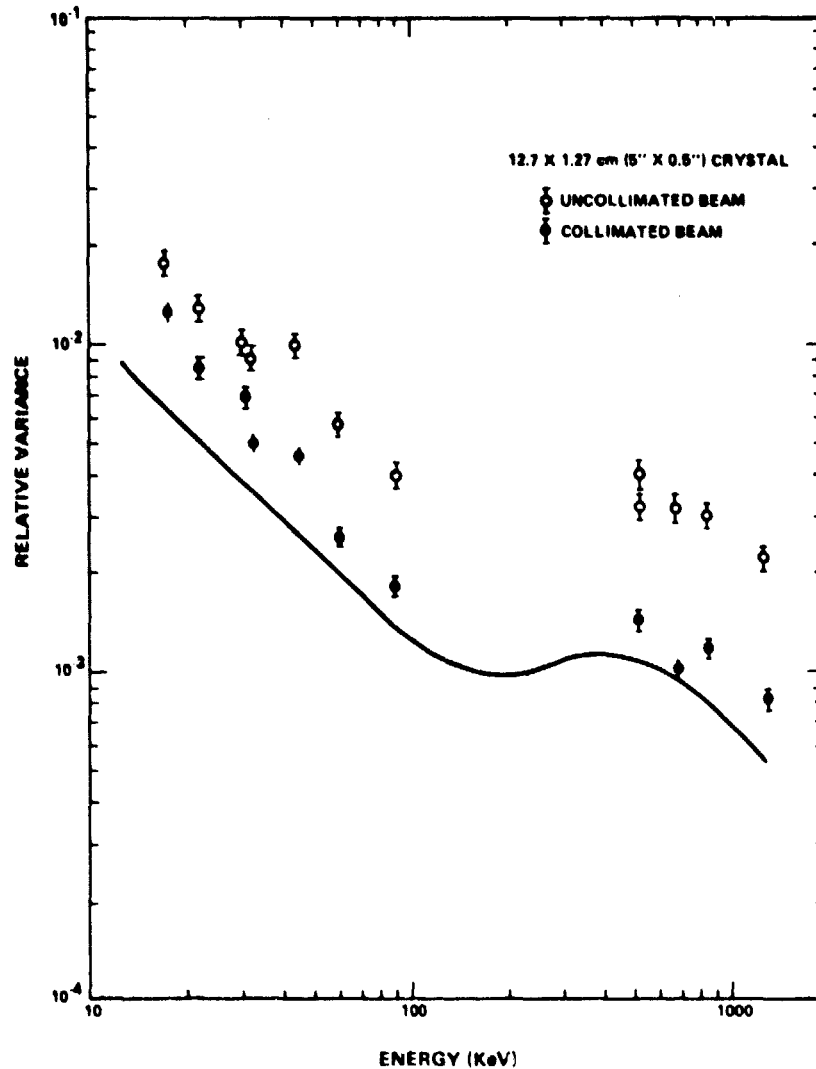
26

Figure 16. Relative variance versus gamma-ray energy for collimated
(solid circles) and uncollimated (open circles) gamma-ray beams
incident on the 12.7 by 1.27 cm (5 by 0.5 in.) crystal. The
line shows a calculation assuming transfer variance $V_T = 0$.

## C. Light Collector Housings

The procedure for testing light collector housings on the 50.8 cm
(20 in.) crystals was described in Section III.C. In a preliminary test,
pulse height and variance of the 88 keV line of Cd^{109} were measured for
six configurations of light collector using an off-the-shelf Bicron crystal.
The six configurations are shown in Figure 17 drawn to scale. Parameters
specifying the geometry are the height h of the PMT plate above the
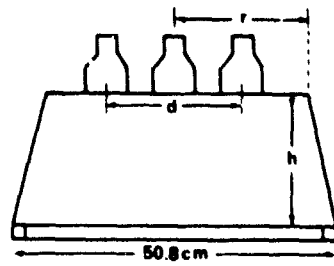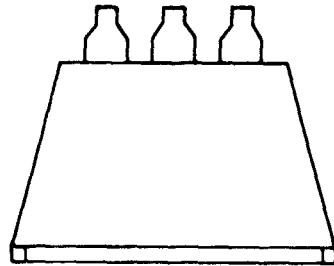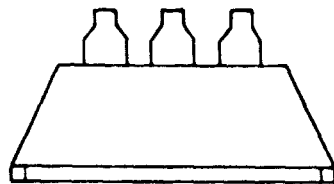
Figure 17. Configurations tested using Bicron off-the-shelf
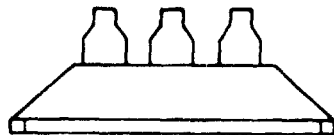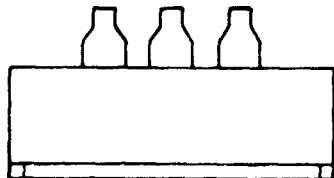crystal (crystal A).

scintillator, the radius r of the PMT plate, and the distance d between tube centers (Fig. 6). The results are presented in Table 3, where geometry parameters, light collection efficiency, and transfer variance are tabulated. The light collection efficiency was determined by comparing the pulse height with that obtained using the 12.7 by 1.27 cm (5 by 0.5 in.) crystal, assumed to have a light collection efficiency of 1. Uncollimated gamma-ray beams were used in all configurations, and collimated beams were also used in most of the configurations.

TABLE 3. LIGHT COLLECTOR HOUSING PERFORMANCE AT 88 keV

Configuration Number	Plate Height h (cm)	Plate Radius r (cm)	Tube Separation d (cm)	Light Collection Efficiency T		Resolution		Transfer Variance	
				Collimated	Uncollimated	Collimated	Uncollimated	Collimated	Uncollimated
1	22	21	21	0.093	0.085	0.40	0.46	0.017	0.026
2	14	24	23		0.088		0.71		0.077
3	31	19	19	0.084	0.080	0.43	0.44	0.019	0.021
4	17	19	19	0.11	0.089	0.44	0.52	0.024	0.036
5	8	19	19	0.11	0.082	0.63	0.82	0.060	0.107
6	17	28	23		0.088		0.53		0.038

The light collection efficiencies are remarkably uniform from one configuration to the next, but very low compared to the 12.7 by 1.27 cm (5 by 0.5 in.) crystal. Because the different geometries had vastly different reflecting surface area, the constancy of the light collection efficiencies implies that the Eastman No. 6080 high-reflectance coating had negligible absorption of light. The low efficiency of light collection ($\sim$ 9 percent) is apparently due to absorption in the crystal. [It is assumed that the luminous efficiency of the 50.8 by 1.27 cm (20 by 0.5 in.) crystal is equal to that of the 12.7 by 1.27 cm (5 by 0.5 in.) crystal]. In fact, a visual inspection of the crystal supports this hypothesis. The 50.8 cm (20 in.) crystal is noticeably greyer than the 12.7 cm (5 in.) crystals. Two further tests of the 50.8 cm crystal were performed. In one test, a PMT was directly coupled to the face of the 50.8 cm crystal with Dow Corning optical coupling compound and illuminated with a collimated beam of 88 keV gamma rays. The light collection efficiency was 0.53. Although some of the light is expected to escape in this geometry, the light collection efficiency is significantly less than that of the 12.7 cm crystal. In another test, the 50.8 cm crystal was replaced by the 12.7 cm crystal placed at the center of a 50.8 cm disc of white styrofoam, using configuration 4 for the light collector housing. The light collection efficiency increased from 0.11 to 0.31 for collimated gamma rays.

The poor optical properties of the 50.8 cm (20 in.) crystals are probably due to absorption of light by the surface of the aluminum container. This surface has a sprayed coat of white paint, rather than the high-reflectance MgO surface of the 12.7 cm (5 in.) crystals. The optical properties of the large crystals are adequate for their intended application as gamma-scan camera plates.

The transfer variance is strongly dependent on light collector geometry. As Table 3 shows, V_T ranges from 0.021 to 0.107. Figure 18 shows a plot of resolution versus distance h from the PMT's to the crystal for an uncollimated beam of 88 keV gamma rays. The resolution improves with increasing distance, leveling off above approximately 20 cm. This dependence is due to a more uniform "view" of the crystal by photomultipliers at greater distance and implies that a significant fraction of the collected light is unreflected after emission from the crystal.
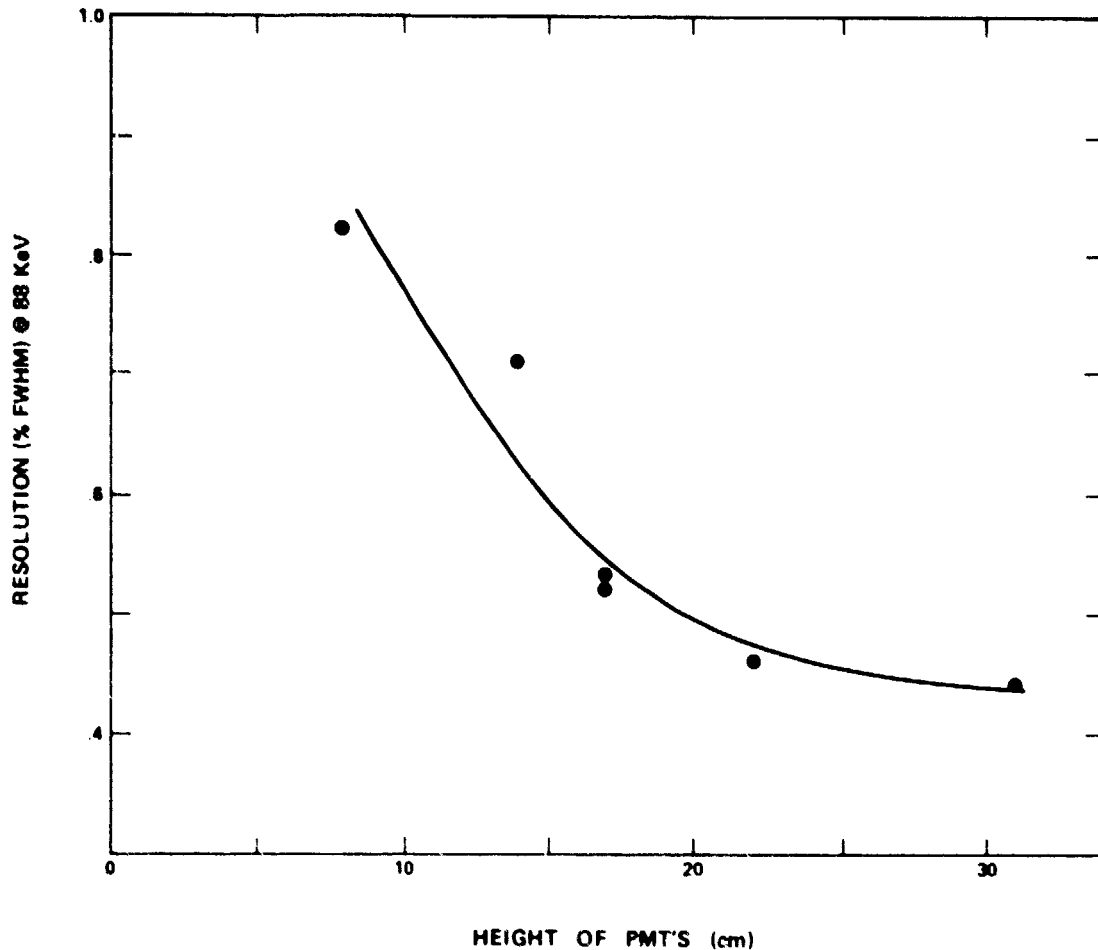

Figure 18. Resolution of 88 keV line versus height of PMT
top plate above crystal for the 50.8 by 1.27 cm
(20 by 0.5 in.) crystal.

After these tests, three additional 50.8 by 1.27 cm crystals were obtained to study their optical properties in our application. The four crystals tested were:

A — Bicron off-the-shelf crystal with painted backing

B — Bicron crystal with high-reflectance paper backing

C — Harshaw crystal with high-reflectance paper backing

D — Harshaw crystal with 0.25 in. Pyrex glass cemented to both sides.

Crystal D was selected for study because it may provide greater mechanical strength. The window on one side of that crystal was covered with Millipore filter paper to act as a light-reflecting surface.

The light outputs of the crystals were compared using a standard cylindrical light collection housing. The height h was 35 cm, plate radius r was 28 cm, and tube separation d was 30 cm. This geometry is not particularly efficient, but the relative light output of the crystals themselves was the focus of this test. Table 4 presents the results using 88 keV gamma rays. Crystal B exhibited the highest system efficiency and the best resolution, but all three of the new crystals were significantly better than the originally tested crystal (crystal A).

Next, a series of tests were undertaken to determine the optimum light collection housing for the crystal with the best optical properties (crystal B). The results from the tests on crystal A are not directly applicable but provided guidance for choosing the designs that are most likely optimum. It should be noted that the best geometry represents a compromise between light collection efficiency and uniformity. Since the statistical variance decreases with energy, a specific design will be optimum at one energy only. We chose to design for best performance at 88 keV because the average energy of BATSE events should be near 88 keV and because a clean 88 keV gamma-ray peak is obtained from Cd^{109}. The source was approximately 60 cm from the crystal, giving uniform illumination to within approximately 20 percent. The configurations tested using crystal B are shown in Figure 19, drawn to scale. In configurations 1 and 2, the housing was a cylinder, permitting any height h, up to 36 cm, to be examined.

Resolution was measured with all three tubes operating and with only two tubes operating. The latter test was made because there is a possibility of PMT or high-voltage power supply failure during the 2-year GRO mission. The results are shown in Figure 20, where resolution is plotted against housing height h. The points below the dashed line at 41 percent resolution represent data taken with three PMT's operating; the points above the line are for two PMT's operating. The different symbols refer to the different configurations shown in Figure 19. The two curves show the trend of the data.

The effect of tube separation d on resolution can be seen by comparing configuration 1 (d = 29 cm) with configuration 2 (d = 23 cm). With all three tubes working, the difference in resolution is slight; but with two tubes only, configuration 2 (with closer tubes) is superior (better resolution), especially at small heights, as might be expected intuitively.

31

TABLE 4. COMPARISON OF OPTICAL PROPERTIES OF 50.8 cm (20 in.) CRYSTALS

Crystal	System Efficiency ϵ (photoelectrons/keV)	Resolution @ 88 keV (%)
A	0.76	48
B	1.05	38
C	0.91	41
D	0.95	41

Figure 20 also shows that the resolution with two tubes degrades seriously for all configurations having height h less than approximately 25 cm. The cone configurations provide better resolution than the cylinders at any value of h. The best configurations were numbers 3 and 5, both tall cones. The best resolution was 32 percent for three tubes and 42 percent for two tubes.

Based on these tests, the optimum geometry for the light collection housings is a cone, 25 to 30 cm high, and a tube separation of approximately 20 cm.

V. CONCLUSIONS

The following is a brief summary of the findings of this study:

EMI type D302B Photomultiplier Tubes

- $V_m = 0.64$

- High voltage ~ 700 V for good resolution

- Cathode to first dynode voltage not critical between 200 and 500 V

- Gain per stage $\propto (HV)^\gamma$, where $\gamma = 0.6$ to 0.7

- Space-charge effects are ~ 5 percent at 1 mA peak anode current and ~ 25 percent at 10 mA

- Bleeder string current must be 60 times average anode current for linearity within 1 percent
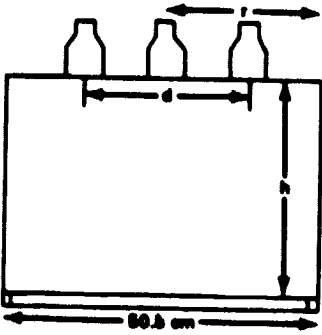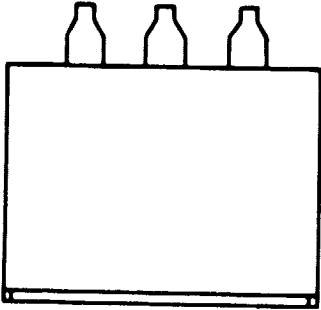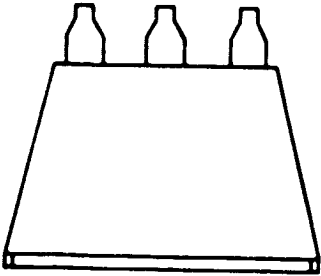
32
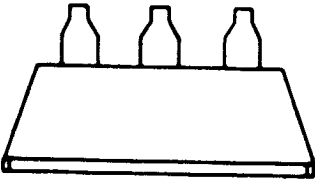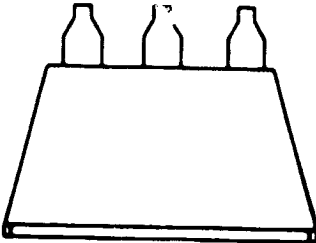
Figure 19. Configuratic...s tested using Bicron crystal with high-reflectance paper backing (crystal B).

Figure 20.   Resolution versus height h of light collector housing
using crystal B .

Sodium Iodide

- With good light collection, 13.9 photoelectrons collected
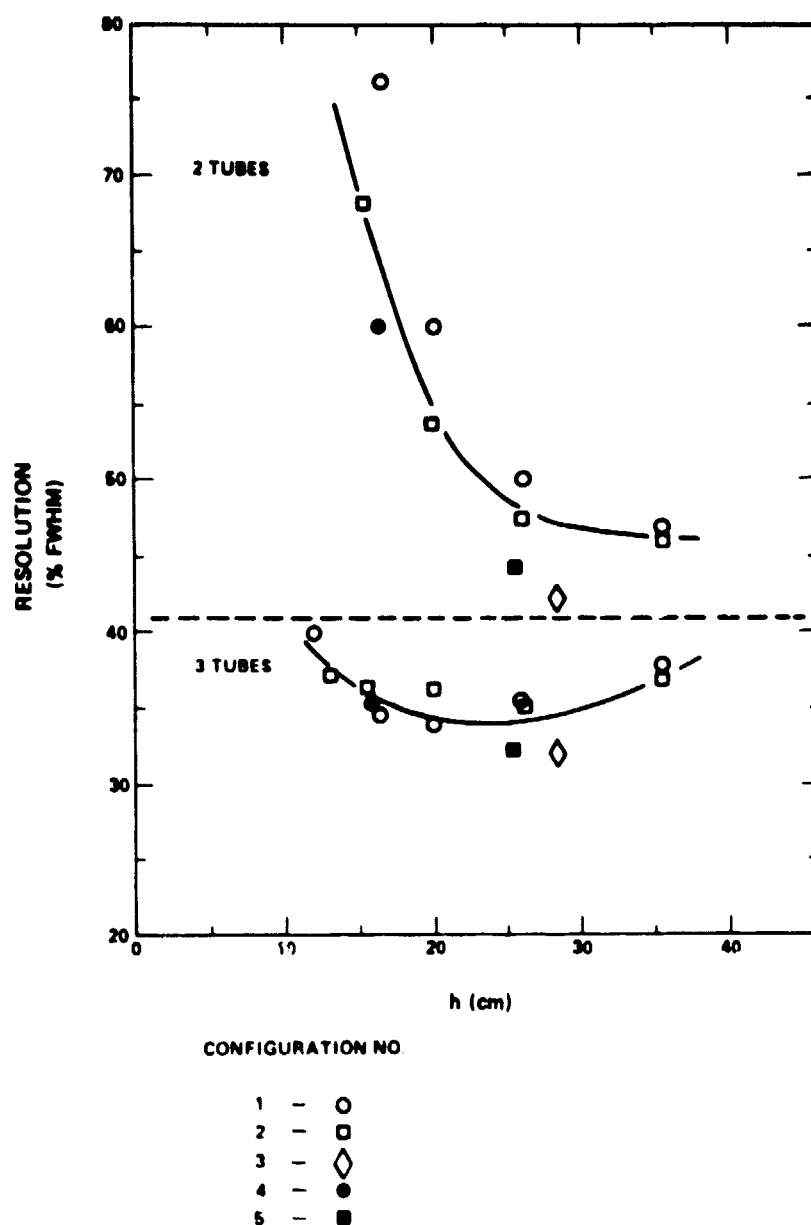 at first dynode per keV deposited (at 662 keV)

- Nonlinearity in agreement with Zerby et al. [15]

34

50.8 cm (20 in.) Crystals and Light Collection Housings

- Bicron crystals with paper reflector had best light output

- Best geometry is a cone of height 25-30 cm, with tubes spaced ∿ 20 cm

- With best geometry, energy resolution at 88 keV is ∿ 32 percent with three tubes operating, and ∿ 42 percent with only two tubes operating.

REFERENCES

1. Brietenberger, E.: Progress in Nuclear Physics. Vol 4, p. 56, Pergamon Press, 1955.

2. Swank, R. K. and Buck, W. L.: Nucleonics, 10, 51, 1952.

3. Prescott, J. R., and Takhar, P. S.: I.R.E. Trans. Nucl. Sci., NS-9 (3), 36, 1962.

4. Parsons, A. J.: Photomultipliers-Space Charge Effects and Transit Time Spread. EMI R/P 064, 1977.

5. Lush. H. J.: J. Sci. Inst., 42, 597, 1965.

6. Land, P. L.: Rev. Sci. Inst., 42, 420, 1971.

7. Kovash, M. A. and Blatt, S. L.: N.I.M., 163, 113, 1979.

8. Kerns C. R.: IEEE Trans. Nucl. Sci., NS-24 (1), 353, 1977.

9. Hiebert, R. D., Thressen, H. A., and Obst. A. W.: N.I.M., 142, 467, 1977.

10. Keene: Rev. Sci Inst., 34, 1220, 1963.

11. Lindow, J. T. et al.: Harshaw Scintillation Phosphors. 1975.

12. Bellian, J. G., and Dayton, R. R.: NaI(Tl) Scintillation Detectors. Bicron Corporation, 1974.

13. Akimov. Yu. K.: Scintillation Counters in High Energy Physics. Academic Press, 1965.

14. Knoll, G. F.: Radiation Detection and Measurement. 1979.

15. Zerby, C. D., Meyer, A., and Murray, R. B.: Nucl. Inst. and Meth., 12, 115, 1961.

16. Iredale, P.: Nucl. Inst. and Meth., 11, 340, 1961.

17. Narayan, G. H., and Prescott, J. R.: IEEE Trans. Nucl. Sci., N.S 15(3). 162, 1968.

18. Clay, R. W. and Gregory, A. G.: Nucl. Inst. and Meth., 153, 467, 1978.

APPENDIX

PROCEDURE FOR DETERMINING SINGLE PHOTOELECTRON SPECTRUM AND MULTIPLICATION VARIANCE

The following procedure is used to determine the spectrum of single photoelectron events and to determine the average pulse height corresponding to one photoelectron:

1) Set up electronics as shown in Figure 4. The PMT must be kept in darkness for several hours before making measurements. Set PHA lower level discriminator to zero and select coincidence mode.

2) ʷ ʰ preamplifier on but with high voltage off, set amplifier gain as high as possible without allowing preamp noise to go above the first channel or two of the PHA. Deadtime from preamp noise must be small.

3) With LED amplitude at zero, turn on high voltage and increase until PMT noise (which is largely due to single photoelectron events) extends approximately 20 to 30 channels. With the EMI 11-stage tubes, approximately 1400 V was found to be satisfactory.

4) Set the PHA livetime to some standard value (500 or 1000 s is satisfactory). Turn the LED amplitude sufficiently high to have an analyzed pulse every trigger. Acquire a spectrum. Integrate the spectrum to determine the total number of triggers per run N_T.

5) Acquire a spectrum with the LED amplitude at zero to obtain the background spectrum. Determine the number of background events per run N_B and save the background spectrum. It is necessary that $N_B \leq 0.1\ N_T$. This criterion may be difficult to achieve with PMT's having less than 11 stages. If the background rate is too high, try a higher voltage on the tube and a lower amplifier gain. If necessary, set lower level discriminator to cut out noise. High backgrounds may also be caused by taking measurements too soon after exposure of the PMT to room lights.

6) While observing amplifier output on the oscilloscope, increase LED pulse amplitude until pulses are occasionally seen. However, keep amplitude low enough that most ($\geq$ 80 percent) of the triggers show no pulse. This requirement ensures that most of the events observed are due to single photoelectrons.

7) Acquire a spectrum, called the background + LED spectrum. Integrate to find the number of events analyzed N_L.

8) The spectrum of LED pulses is obtained by subtracting the background spectrum from the background + LED spectrum and correcting for deadtime. The background spectrum is corrected by multiplying by $(1 - f_L)$, where f_L is the fraction of triggers in which an LED pulse is present and is found from the equation

$$f_L = \frac{N_L - N_B}{N_T - N_B} .$$

This correction, which accounts for those triggers during which a background and an LED pulse are present, can be made easily on the TN 1710 PHA by using the multiply feature of the Data Processor Module. The validity of the background subtraction is assured if the first channel is high in the background spectrum and the background + LED spectrum due to preamp noise, but lies on a smooth curve in the LED spectrum.

9) Compute the average channel number $\bar{x}$ of the LED spectrum.

10) The LED spectrum is not equivalent to the single photoelectron spectrum, since there is occasionally more than one photoelectron per LED pulse. The average number of photoelectrons per analyzed pulse $\bar{n}_{pe}$ is determined from the known rate of triggers in which at least one photoelectron is present. From Poisson statistics, it can be shown that

$$\bar{n}_{pe} = - \frac{\ln (1 - f_L)}{f_L} .$$

As $f_L \to 0$, $\bar{n}_{pe} \to 1$, and the LED spectrum asymptotically approaches the single photoelectron spectrum.

11) Determine the average channel for single photoelectrons x_1 from the equation $x_1 = \bar{x}/\bar{n}_{pe}$. Additional runs should be made at various LED pulse amplitudes to verify that x_1 is insensitive to amplitude. For $f_L \ll 1$, statistical errors in $\bar{x}$ become large. As $f_L \to 1$, statistical errors in $\bar{n}_{pe}$ become large.

The multiplication variance V_m can now be determined using the same experimental setup. The procedure is as follows:

38

1) Increase the pulse generator amplitude until an LED pulse is present every trigger ($f_L = 1$).

2) Acquire a spectrum and determine the variance V and mean channel number $\bar{x}$ of the pulse height distribution. For sufficiently large LED pulses, the spectrum is approximately Gaussian. In this case, the peak channel may be used for the mean, and the FWHM may be used to find the relative variance from the equation

$$V = \frac{(FWHM)^2}{2.354\,\bar{x}} \quad .$$

3) From the mean channel number $\bar{x}$ determine the mean number of photoelectrons $\bar{n}_{pe} = \bar{x}/x_1$.

4) Determine the multiplication variance from

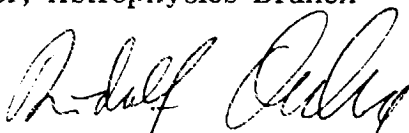$$V_m = V_s\,\bar{n}_{pe} - 1 \quad .$$

APPROVAL

PERFORMANCE OF PHOTOMULTIPLIER TUBES AND SODIUM IODIDE SCINTILLATION DETECTOR SYSTEMS
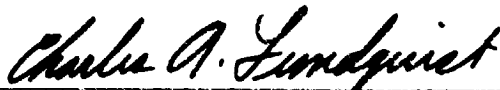
By Charles A. Meegan

The information in this report has been reviewed for technical content. Review of any information concerning Department of Defense or nuclear energy activities or programs has been made by the MSFC Security Classification Officer. This report, in its entirety, has been determined to be unclassified.

THOMAS A. PARNELL
Chief, Astrophysics Branch

RUDOLF DECHER
Chief, Space Physics Division

CHARLES A. LUNDQUIST
Director, Space Sciences Laboratory

40